International Journal of Multiphysics
Volume 18, No. 2, 2024
ISSN: 1750-9548

Prediction of Loess Collapsibility Coefficient through the HHO-BP Neural Network

Yanqing Wei[1], Erqiang Li[1*], Paul Archbold[2], Brian Mullarney[2], Jiajia Li[3], and Bing Xie[1]

[1]Department of Civil Engineering, Luoyang Institute of Science and Technology, Luoyang, Henan, 471000, China

[2]School of Engineering & Materials Research Institute, Technological University of the Shannon, Westmeath, N37HD68, Ireland

[3]China Construction Seventh Engineering Bureau Co., LTD, Zhengzhou, Henan, 450000, China

*Corresponding Author.

Abstract

The coefficient of collapsibility is the key parameter involved in the computation of the loess collapsible deformation. However, influencing by many factors, theoretical estimation of this parameter becomes extremely difficult. In order to quickly and conveniently predict the loess collapsibility coefficient according to soil index properties, through data mining technology, a model was proposed based on BP neural network optimized by HHO (Harris Hawk Optimization) algorithm. The proposed model was validated using a database acquired from engineering practice, which indicated that at least five soil index properties were necessary for accurate predictions. Also, compared with prediction models based on BP (Back Propagation) and PSO (Particle Swarm Optimization)-BP neural network, the proposed model gained faster iteration rate, higher prediction accuracy and lower error value. Sensitivity analysis based on the connection weights shows that the most important index properties affecting the coefficient of collapsibility are plasticity index and void ratio, followed by dry density and degree of saturation, and finally water content.

Keywords: Collapsible loess; Coefficient of collapsibility; BP neural network; HHO algorithm

1. Introduction

The loess as a typical problem soil is widely distributed, the northwestern and central USA, northern Russia, interior Alaska and south America [1-3]. In China, 6% of the territory is covered by loess, 60% of which belongs to problematic soil of high collapsibility [4]. Collapsible loess is typically in a state of unsaturated condition. Due to the function of matric suction, the original stable inner structure of collapsible loess could be maintained [5]. However, upon water intrusion induced by precipitation, together with matric suction reduction, the collapsible loess would suffer remarkable collapsible settlement due to soil inner structure collapse[6-7]. Sometimes significant collapsible deformation may give rise to serious engineering problems. For example, it was reported that 1505 buildings and 80 kilometers of underground pipes were damaged due to collapsible deformation in China during the period of 1974 to 1975 [8]. Therefore, the estimation of the collapsible deformation of collapsible loess has been a research focus in recent years.

Coefficient of collapsibility (δ_z), as the ratio of $\triangle$h (i.e., difference of soil sample height between natural and saturated states under vertical pressure of 200kPa) to h0 (i.e., initial height of the soil sample), has been widely used in engineering practice to evaluate the degree of collapse of loess and estimate the amount of collapsible

deformation simply and intuitively [9]. Generally, this parameter is determined through indoor immersion compression test on undisturbed soil. However, sometimes the collection of undisturbed soil sampling is time-consuming and costly. The sample is easy to be disturbed as well. All these factors may lead to large errors in the test results [4,10]. Instead, researchers began to work on theoretical or empirical models to make reasonable estimations of loess collapsibility coefficient. Generally, these models could be categorized into two types. The first one is based on regression analysis, which initially collects the key factors influencing the coefficient of collapsibility (i.e., mineral composition, pore structure, stress state, etc.) and then establishes a prediction model using mathematical statistical methods [11-15]. The second one is based on neural network, which commonly uses a nonlinear intelligent algorithm to learn and predict the fuzzy relation between the loess physical properties indexes and coefficient of collapsibility, thus making evaluations quickly and concisely [16-19]. The regression analysis methods are able to establish a clear functional relation between the coefficient of collapsibility and the loess's physical properties for certain region. However, the correlation coefficient of predictions just ranged from 0.7-0.9 [20-21]. Such precision of predictions sometimes cannot meet the requirement of engineering applications. The existing literature shows that the neural network model is highly consistent with the nonlinear correlation between the soil physical property index and loess's coefficient of collapsibility, especially BP neural network model [22-25]. However, this model has the disadvantages of slow convergence speed. Also, it would fall into local optimization easily, which limits the accuracy of prediction.

The HHO (Harris Hawk Optimization) algorithm is able to overcome the shortcomings of the traditional BP neural network by finding the neural network's optimal solution of the initial connection weights and thresholds. Due to these advantages, in this study, a model was proposed for estimations of the loess collapsibility coefficient based on the BP neural network optimized using the HHO algorithm. By analyzing the inherent mechanism of the collapsible deformation, five basic soil index properties (i.e., degree of saturation, water content, dry density, void ratio, and plastic index) were selected to develop the prediction model, which also enabled the proposed method to be applied universally in different regions. Comparative analysis among BP neural network based model, PSO (Particle Swarm Optimization) -BP neural network based model and four-parameter HHO-BP neural network based model indicated that the five-parameter HHO-BP neural network based model was capable of predicting the loess coefficient of collapsibility in higher speed and accuracy.

2. The HHO-BP Neural Network based Model for Collapsibility Coefficient Prediction

In this part, initially the inherent mechanisms of the loess collapsible deformation were analyzed. The key soil index properties influencing the loess collapse were determined. Then the traditional BP neural network was optimized using the HHO algorithm by optimizing the initial connection weights and thresholds. By introducing the key soil index properties into the input layer and setting the coefficient of collapsibility as the final output layer, the prediction model could be developed based on data mining technology.

2.1 Soil index properties related to the loess collapsible deformation

Figure 1 illustrate the mechanism of the collapse deformation under water intrusion. As shown in Figure 1(A), in natural unsaturated condition, there are both air and water inside the soil pores. Soil aggregates were connected to each other through either direct or indirect point and surface contact. Apparently the void ratio (e) which indicates the pore volume inside the soil, fundamentally determines the amount of possible collapsible deformation. While the amount of soil aggregate inside the soil is represented by the dry density (ρ_d), which represents the content of solid soil particles inside the soil. For indirect point and surface contact, clay particles act as the joint between adjacent soil aggregates. These joints are also referred to as the weak zone since they would soon rupture and dissolve under water intrusion. The amount of clay particles inside the soil is manifested by the plasticity index (I_p). Together with the surface tension, which acts as the bonding force exerted by water menisci of the close air bubble, the initial inner soil structure is maintained. The surface tension is manifested by matric suction, which is related to the water content (w) and degree of saturation(S_r). While as water infiltrates into the loess, as shown in Figure 1(B), the big weak zone ruptures and the small weak zone disappears. The soil aggregate composed of silts breaks into separated soil particles. Also, the surface tension generated by the air bubble vanishes. Under the combined function of these factors, the initial soil structure cannot be maintained

any longer. As a consequence, under the soil self-weight or the vertical load, the broken loess particles and discrete clay particles fill the original pores inside the soil structure, resulting in soil volume reductions [26-28], as shown in Figure 1(C)

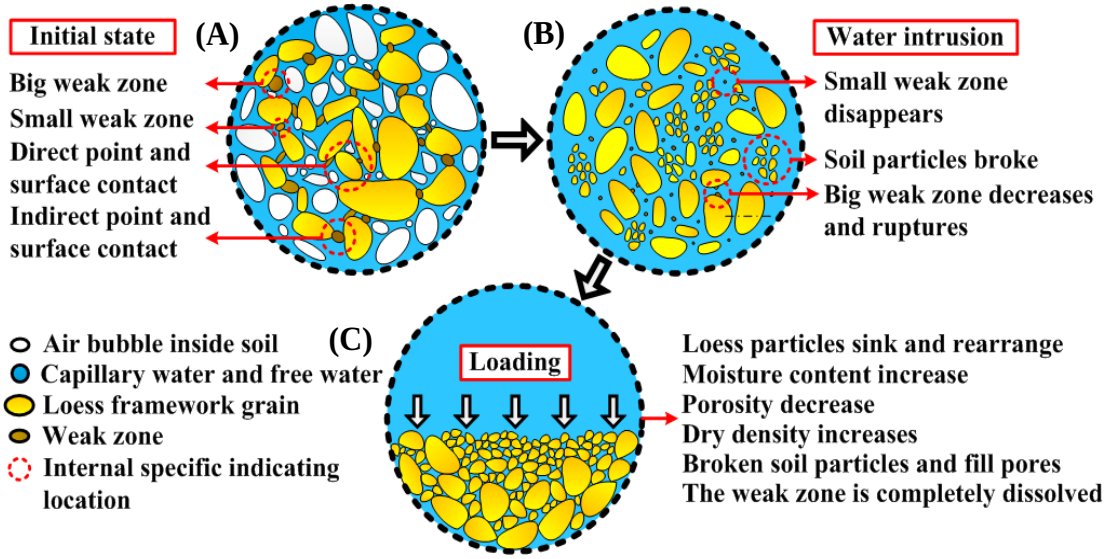

Figure 1 Mechanism of the loess collapsible deformation

Besides the five soil index properties as analyzed above, scholars also concluded some other factors related to the coefficient of collapsibility, such as the liquid limit, plastic limit and unit weight, etc [29-31]. However, these factors generally signify the same content as the aforementioned soil index properties. For example, the liquid limit and plastic limit signify the clay content inside the soil, while apparently they are less representative compared with plasticity index. Similarly, the unit weight intending to signify the content of solid soil particles inside the soil is not representative than dry density. For this reason, the void ratio(e), dry density(ρ_d), plasticity index(I_p), water content(w) and degree of saturation(S_r) are selected as the input parameters in the prediction model of the collapsibility coefficient.

2.2 The prediction model based on BP neural network optimized using the HHO algorithm

The prediction model based on BP neural network optimized using HHO algorithm was developed following a three-step-procedure. Initially the neural network structure was built in a similar way to the BP neural network, which determined the number of neurons and various functions. Then the thresholds in input layer, hidden layer and output layer as well as the connection weights between different layers were initialized. In this process, the initial thresholds and connections weight inside the BP neural network were optimized using the HHO algorithm, so as to significantly improve the prediction performance. Finally, the neural network was train by the training data set so as to fit the parameters in the prediction model.

More specifically, as shown in Figure 2, the neural network structures were composed of three layers, namely the input layer (i.e., soil index properties), hidden layer and the output layer (i.e., coefficient of collapsibility). Then a series of networks were built between input layer and hidden layer as well as the hidden layer and the output layer. There was a self-feedback threshold in the input layer while there were mutual feedback weights between the input and hidden layers, and between the hidden and output layers. For traditional BP neural network, the specific structural characteristics caused that minor changes in each node's threshold and connection weights could significantly affected the output results. In other words, the randomness in initial thresholds and connection weights resulted in low convergence speed and poor prediction accuracy.

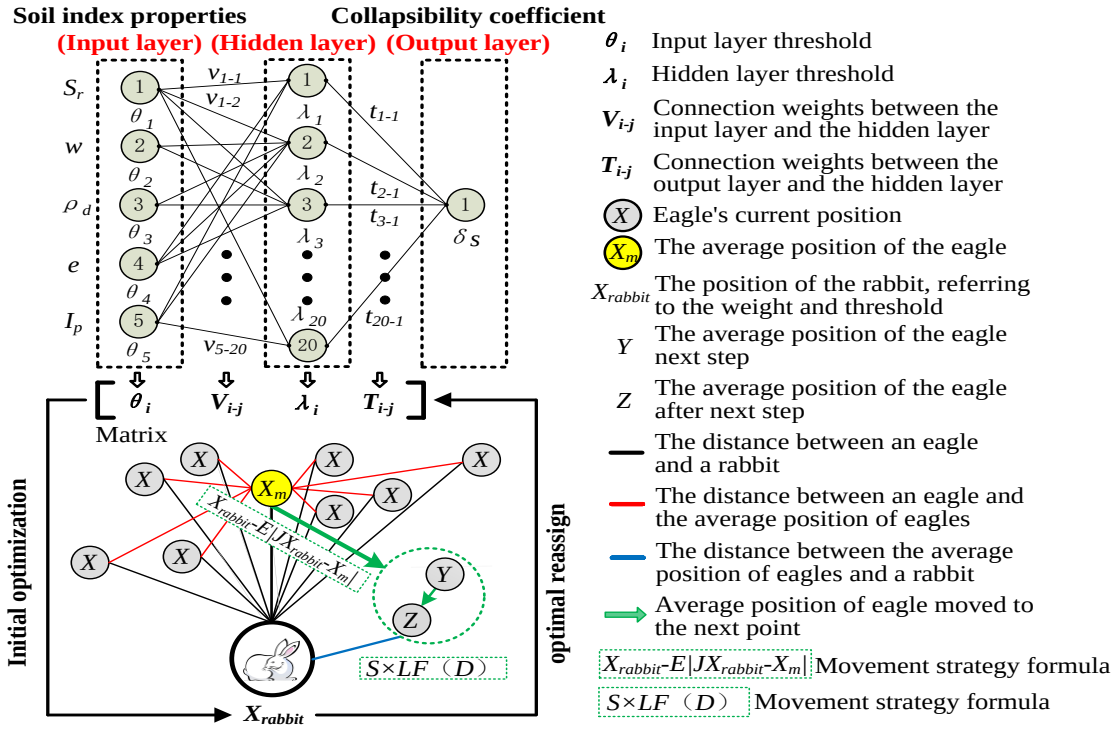

Figure 2 The schematic of the proposed prediction model

The HHO algorithm was a population-based and free-gradient optimization technology which simulated the cooperative behavior of the Harris Hawk to achieve efficient optimization [32]. It is always used to provide high accuracy in extracting the optimal parameters and enhanced the prediction performance [33]. In order to improve the convergence speed and prediction accuracy, the BP neural network was optimized with the assistance of the HHO algorithm following a six-step-procedure:

(1) Use the thresholds and connection weights to be optimized as the HHO algorithm's individual dimension. As shown in Figure 2, the X_{rabbit} is referred to as the thresholds and connection weights in the BP neural network structure, for example θ_{ij}, V_{ij}, λ_{i-j}, T_{i-j};

(2) According to the number of parameters to be optimized, determine the prey's dimensionality and authorize the initial values of the prey energy, the number of Hawks and the position parameters;

(3) Consider the mean square error between the predicted and actual value (as shown in Eq.1) as the neural network's fitness function;

$$f_{obj} = \frac{1}{M}\sum_{i=1}^{M}(X(i)-x(i))^2 \tag{1}$$

where M is the number of samples in the training set; X(i) is the neural network model's predicted value of the i-th sample; x(i) is the actual value of the i-th sample.

(4) Use the HHO algorithm's initialization assignment to generate the initial connection weights and thresholds randomly and store them in the matrix unit best_X, and the initial fitness value is recorded in the matrix unit Rabbit Energy;

(5) Use Eq.(2) and Eq.(3) to update the Hawk group's position continuously, then calculate the fitness continuously. Compare the updated fitness value with the original one. If the updated fitness value is smaller than the original value, then store the updated value in the matrix unit best_X and Rabbit_Energy to replace the original one;

$$X(t+1) = \Delta X(t) - E\left|JX_{rabbit}(t) - X(t)\right| \tag{2}$$

$$X(t+1) = X_{rabbit}(t) - E\left|\Delta X(t)\right| \tag{3}$$

In which: $X(t+1)$ and $X(t)$ denote the positions of the Harris Hawk at the $t+1$ and t iterations, respectively; X_{rabbit} is the position of the prey selected randomly; E is the prey's energy; $\Delta X(t)=X_{\text{rabbit}}(t)-X(t)$, $J=2[1-r_5]$ is a random number between [0,2] that represents the random jump intensity when the prey escapes; r_5 represents a random number in the range of [0,1], and $\Delta X(t)$ denotes the difference between the prey's position vector and the current position.

(6) The aforementioned update continues until the default accuracy (i.e., e^{-7}) or the default iteration number is reached (i.e., 2000).

Then the optimal initial connection weights and thresholds values was introduced back into the BP neural network, after training using the training data set, the proposed model is capable of predicting the collapsibility coefficient through certain soil index properties. Figure 3 illustrates the flowchart of the neural work for collapsibility coefficient prediction. In this study, the BP neural network adopted a single hidden layer model with a structure of 5(input layer)-20(hidden layer)-1(output layer). The number in the algorithm population was set to 10 and the improved HHO algorithm was iterated for 100 times.

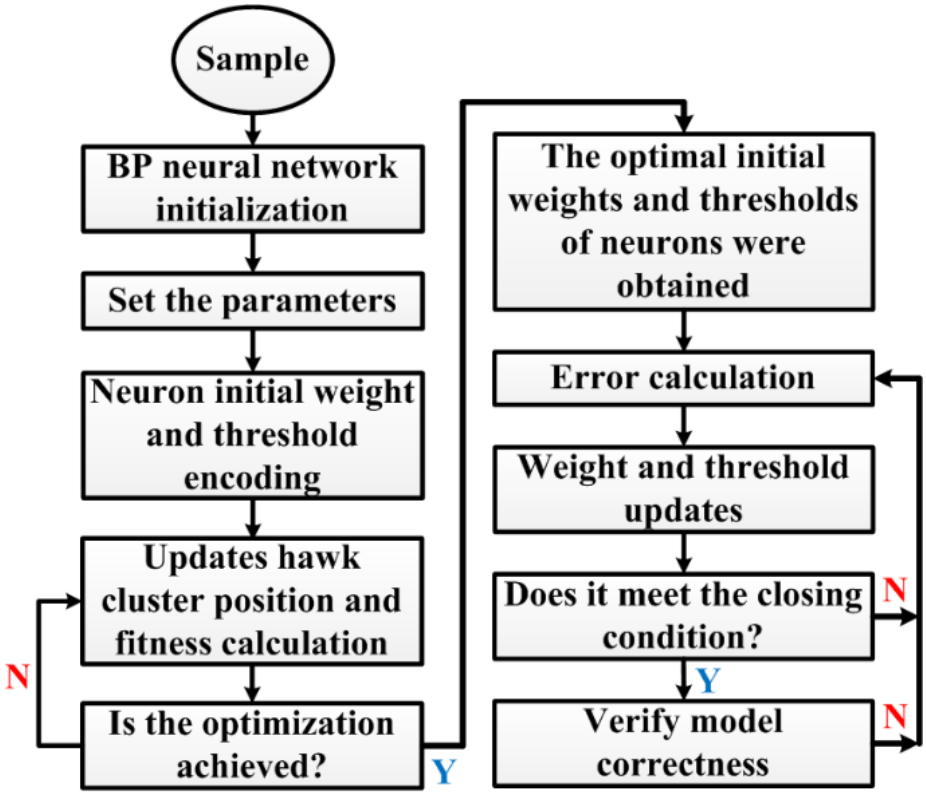

Figure 3 Flowchart of the BP neural network optimized using the HHO algorithm

3. Case Study

In this section, the feasibility of the proposed prediction model was validated using a database presented by An's [22], Feng's [23], Wang's[34], Ding's[35], Liu's[36] and Han's[37], who collected totally 80 groups of data of soil index properties and collapsibility coefficient in Lanzhou and Shanxi, China. The data base was divided into the training set which contained 60 groups of data and the testing set which contained 20 groups of data. The detained data base was available in Table1.

Table 1 The coefficient of Collapsibility data base[22,23,34-37]

No.	S_r/1	w/%	ρ_d/kg/m^3	e/1	I_p/%	δ_s/1	No.	S_r/1	w/%	ρ_d/kg/m^3	e/1	I_p/%	δ_s/1

1	36.84	15.5	1.260	1.136	15.9	0.044	41	50.80	17.3	1.410	0.919	16.90	0.007
2	32.62	13.9	1.260	1.151	16.2	0.046	42	15.72	6.8	1.250	1.168	16.40	0.027
3	24.40	11.4	1.190	1.262	16.2	0.073	43	21.45	9.0	1.270	1.133	16.20	0.013
4	13.27	5.2	1.310	1.058	16.4	0.078	44	12.90	5.2	1.290	1.089	16.20	0.024
5	17.47	7.2	1.280	1.113	16.7	0.078	45	19.35	7.6	1.310	1.065	16.50	0.070
6	20.36	8.6	1.260	1.140	16.3	0.080	46	21.37	8.4	1.310	1.001	16.70	0.080
7	27.72	11.5	1.270	1.120	16.5	0.066	47	25.83	10.2	1.310	1.066	16.40	0.056
8	30.25	12.0	1.300	1.071	16.8	0.062	48	30.43	11.5	1.340	1.020	16.10	0.059
9	34.85	13.0	1.350	1.007	16.9	0.059	49	36.14	13.4	1.350	1.001	16.20	0.036
10	37.44	13.8	1.350	0.995	17.0	0.031	50	41.89	15.5	1.350	0.999	16.60	0.021
11	39.77	14.2	1.370	0.964	16.8	0.018	51	41.55	14.8	1.380	0.962	16.70	0.010
12	43.53	15.5	1.380	0.961	16.6	0.017	52	64.50	23.00	1.408	0.950	9.40	0.012
13	48.12	16.6	1.400	0.931	17.0	0.013	53	51.80	17.80	1.418	0.920	7.80	0.010
14	34.93	14.2	1.290	1.098	16.1	0.051	54	53.70	20.00	1.367	1.000	8.50	0.015
15	32.87	12.9	1.310	1.065	16.3	0.043	55	54.10	17.70	1.418	0.820	8.40	0.007
16	29.85	12.0	1.290	1.086	16.4	0.047	56	41.00	15.70	1.347	1.030	8.10	0.034
17	21.01	8.5	1.290	1.093	16.2	0.065	57	47.10	16.90	1.398	0.970	9.10	0.009
18	22.05	9.0	1.280	1.102	16.7	0.063	58	70.90	22.40	1.480	0.850	9.40	0.001
19	21.93	8.8	1.300	1.083	16.2	0.066	59	73.70	23.40	1.480	0.850	9.10	0.001
20	25.07	10.0	1.300	1.077	16.4	0.060	60	34.00	13.10	1.347	1.040	9.30	0.044
21	26.39	10.3	1.310	1.054	16.2	0.049	61	33.00	12.90	1.337	1.050	9.50	0.040
22	29.76	11.0	1.350	0.998	16.6	0.031	62	37.00	14.00	1.357	1.020	9.60	0.035
23	34.51	12.2	1.380	0.954	16.7	0.018	63	34.00	12.10	1.388	0.960	8.70	0.037
24	42.09	14.8	1.390	0.949	16.6	0.016	64	40.00	13.60	1.439	0.900	7.80	0.022
25	47.92	16.5	1.400	0.930	17.0	0.013	65	35.00	10.80	1.480	0.840	7.20	0.007
26	9.47	4.4	1.200	1.255	16.2	0.043	66	28.00	9.20	1.449	0.880	7.50	0.004
27	18.50	8.2	1.230	1.197	15.9	0.027	67	68.00	18.40	1.582	0.730	7.00	0.003
28	11.33	4.8	1.260	1.144	16.4	0.051	68	41.60	16.00	1.347	1.030	8.60	0.036
29	14.04	5.2	1.350	1.000	16.5	0.071	69	36.00	15.00	1.276	1.160	9.40	0.054
30	17.23	7.2	1.270	1.128	16.2	0.074	70	51.00	14.00	1.571	0.730	6.30	0.002
31	16.41	6.6	1.290	1.086	15.9	0.080	71	34.00	10.60	1.480	0.850	7.10	0.005
32	18.18	7.3	1.300	1.084	16.7	0.077	72	44.00	17.10	1.320	1.061	10.9	0.052
33	20.62	7.8	1.340	1.021	16.4	0.078	73	34.00	13.00	1.340	1.021	9.80	0.035
34	26.81	10.5	1.310	1.058	16.6	0.074	74	35.00	13.30	1.330	1.026	9.90	0.041
35	23.60	9.0	1.330	1.030	16.9	0.077	75	27.00	10.90	1.290	1.019	9.90	0.081
36	31.01	11.2	1.370	0.975	16.9	0.057	76	26.00	10.00	1.330	1.034	9.80	0.019
37	34.92	12.6	1.370	0.974	16.90	0.043	77	42.30	20.9	1.140	1.340	12.0	0.087
38	37.09	13.4	1.370	0.975	16.70	0.027	78	50.50	20.4	1.280	1.099	13.4	0.054
39	41.96	15.0	1.370	0.965	16.80	0.018	79	62.00	24.70	1.302	1.090	13.0	0.017
40	46.51	16.4	1.380	0.952	17.00	0.019	80	36.00	15.60	1.220	1.168	10.6	0.058

In order to highlight the advantages of the proposed model based on BP neural network optimized using HHO algorithm, comparisons were made among experimental data and predictions made by proposed model, traditional BP neural network and BP neural network optimized using PSO algorithm. As shown in Figure 4 and Table 2, apparently the best comparisons could be achieved between the true value and predictions made by the model proposed in this study. Also, as shown in Table 3, the coefficient of determination (R^2), the root mean square error (RMSE) and mean absolute error (MAE) were selected to evaluate the performance of three models discussed above. Corresponding equations were listed in Eq.(4) to (6), respectively. The HHO-BP algorithm's optimization accuracy was far higher than the BP neural network and PSO-BP neural network. Further, the HHO-BP algorithm's training speed was higher than the PSO-BP algorithm.

$$R^2=\frac{(n\sum_{i=1}^{n}y_i'y_i-\sum_{i=1}^{n}y_i'\sum_{i=1}^{n}y_i)^2}{\left[n\sum_{i=1}^{n}y_i'^2-(\sum_{i=1}^{n}y_i')^2\right]\left[n\sum_{i=1}^{n}y_i^2-(\sum_{i=1}^{n}y_i)^2\right]} \tag{4}$$

$$RMSE=\sqrt{\frac{1}{n}\sum_{i=1}^{n}(y_i'-y_i)^2} \tag{5}$$

$$MAE=\frac{1}{n}\sum_{i=1}^{n}\left|y_i'-y_i\right| \tag{6}$$

Where n is the number of samples; y' is the prediction made by proposed model; y is the experimental date. The closer R^2 is to 1, and the closer RMSE and MAE are to 0, indicating that the prediction accuracy of this model is higher [38-39].

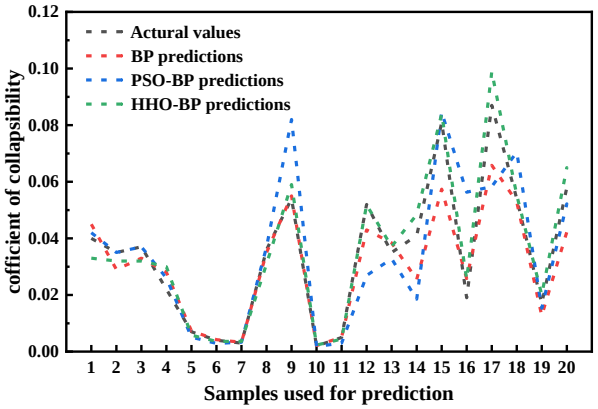

Figure 4 Comparisons of coefficient of collapsibility among BP, PSO-BP and HHO-BP neural network predictions in test set

Table 2 Coefficient of collapsibility of neural network models in test set

Test set NO.	$\boldsymbol{\delta_s}$ Actual values	$\boldsymbol{\delta_s}$ Prediction values of BP	$\boldsymbol{\delta_s}$ Prediction values of PSO-BP	$\boldsymbol{\delta_s}$ Prediction values of HHO-BP
1	0.0400	0.0450	0.0420	0.0330
2	0.0350	0.0290	0.0350	0.0320
3	0.0370	0.0330	0.0370	0.0320
4	0.0220	0.0280	0.0260	0.0300
5	0.0070	0.0073	0.0051	0.0058
6	0.0040	0.0042	0.0029	0.0036
7	0.0030	0.0033	0.0033	0.0036
8	0.0360	0.0350	0.0370	0.0310
9	0.0540	0.0550	0.0820	0.0590
10	0.0020	0.0021	0.0018	0.0023
11	0.0050	0.0051	0.0030	0.0044
12	0.0520	0.0430	0.0269	0.0518
13	0.0350	0.0384	0.0328	0.0371
14	0.0410	0.0255	0.0185	0.0484
15	0.0810	0.0574	0.0846	0.0840
16	0.0190	0.0258	0.0563	0.0255
17	0.0870	0.0658	0.0583	0.0988
18	0.0540	0.0529	0.0705	0.0553
19	0.0170	0.0127	0.0153	0.0201
20	0.0580	0.0423	0.0522	0.0650

Table 3 Comparison of prediction effects of neural network models

Predictive model	R^2		MAE		RMSE		CPU time/s
	Training set	Test set	Training set	Test set	Training set	Test set	Training set
BP neural network	0.685	0.903	0.0107	0.0062	0.0018	0.0094	2.15
HHO-BP	0.751	0.972	0.0097	0.0039	0.0132	0.0050	69.49
PSO-BP	0.741	0.675	0.0084	0.0092	0.0106	0.0150	119.27

Comparisons of the prediction error for all testing data among HHO-BP neural network, BP neural network, and PSO-BP neural network were shown in Figure 5. The HHO-BP neural network's error was significantly less than those of the PSO-BP and BP neural networks. The relative error of the HHO-BP neural network based prediction model fluctuated near zero line, and the fluctuation frequency was small.

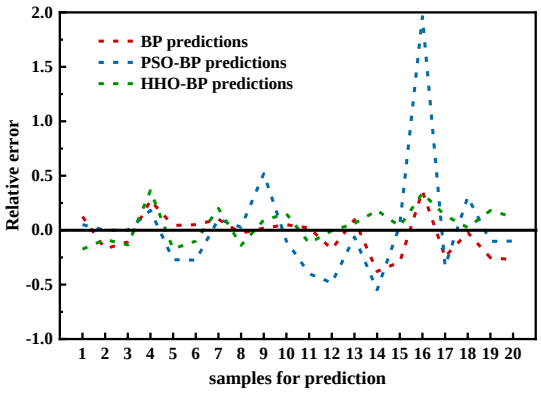

Figure 5 Comparisons of relative errors among BP, PSO-BP and HHO-BP neural network predictions

Figure 6 showed the convergence rate of the predictions made by HHO-BP neural network based model. The fitness fell sharply in the early stage of convergence, while this trend slowed down after around 20 iterations. After 100 iterations, HHO-BP algorithm was able to converge stably.

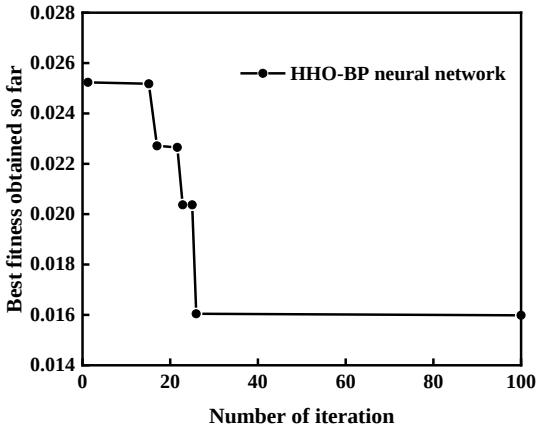

Figure 6 Convergence rate of the HHO-BP neural network prediction

In order to determine the number of soil index properties necessary to produce reasonable predictions, predictions using five soil index properties (i.e., the proposed model) and four soil index properties were made and compared. As shown in Table 4 and Figure 7, the average value of R^2 between the predicted and the actual value by the five-parameter prediction model reached approximately 91%, which was significantly higher than the four-parameter prediction model (approximately 70%). Such a comparison indicated that to predict the

coefficient of collapsibility reasonably, at least five soil index properties were necessary. Further, for other index evaluating the performance of various models, such as the maximum value of R^2, RMSE and MAE, five-parameter model was greater than the four-parameter model.

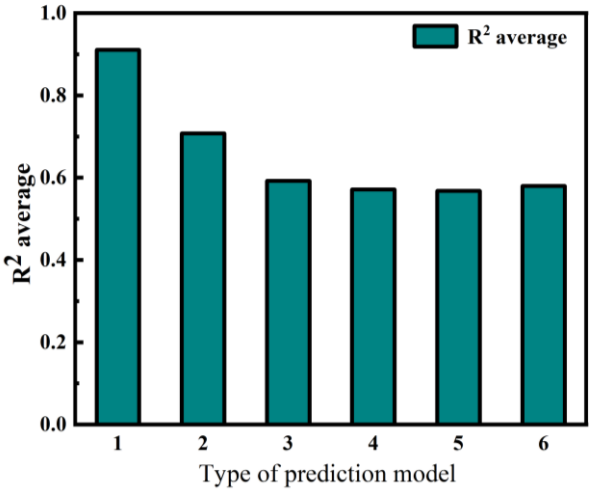

Figure 7 Comparisons of R2 average among five-parameters and four-parameters neural network predictions

Table 4 Comparison of the average prediction effect of HHO-BP neural network model with five-parameters and four-parameters

Parameter settings	**1: Five parameters**		**2: Four parameters（without S_r）**		**3: Four parameters（without e）**		**4: Four parameters（without ρ_d）**		**5: Four parameters（without I_p）**		**6: Four parameters（without w）**	
Collection model	Train-ing set	Test set	Training set	Test set	Training set	Test set	Training set	Test set	Training set	Test set	Training set	Test set
R^2 average	0.7173	0.9105	0.7144	0.7080	0.7184	0.5926	0.7202	0.5712	0.7075	0.5681	0.7076	0.5798
R^2 max	0.8662	0.9716	0.8581	0.944	0.8046	0.9397	0.8174	0.9501	0.8139	0.9004	0.8128	0.9343
RMSE	0.00005	0.0005	0.0002	0.0006	0.0005	0.0035	0.0012	0.0005	0.0004	0.0007	0.0005	0.0009
MAE	0.0073	0.0068	0.0067	0.0084	0.0068	0.0071	0.0070	0.0054	0.0071	0.0074	0.0069	0.0068

4. Sensitivity Analysis

Sensitivity analysis is a technical approach to assess a model's robustness based upon the prediction results. The sensitivity of the proposed model was analyzed according to the connection weights. Corresponding principle is that the greater the sum of the absolute values of the input parameters' connection weights, the greater influence those parameters pose on the output results. The formula to calculate the connection weight was given in Eq. (7). The sensitivity analysis results were shown in Table 5. The connection weights showed that the void ratio and plasticity index were of greater importance. The correlation between the degree of saturation and loess coefficient of collapsibility was greater than water content, and the correlation between the void ratio and coefficient of collapsibility was greater than dry density, which was consistent with the research results presented by Zhang et al. [40].

$$I_X = \left| \sum_{Y=1}^{M} HB_{XY} \right| \tag{7}$$

Where I_x is the sum of connection weights of input neurons to output parameters, HB_{xy} is the connection weights of neurons at each layer, M is the number of connection weights.

Table 5 Sensitivity analysis of parameters

NO. of parameters	Input parameters	Connection weights	
		Absolute value of parameter weights	Ranking
1	*e*	2871.84	1
2	I_p（%）	1283.37	2
3	ρ_d（kg/m^3）	1056.01	3
4	S_r	990.20	4
5	*w*（%）	901.40	5

5. Conclusion

In engineering practice, data mining technology has been widely used to predict the collapsibility coefficient of loess quickly and conveniently based on the site investigation report. However, for commonly used data mining techniques like BP neural network, generations of random thresholds and connections weights may lead to low convergence speed and poor accuracy. In order to solve this problem, in this study, initially soil index properties tightly related to collapsibility coefficient were revealed. Then a prediction models was proposed based on the BP neural network optimized using HHO algorithm. Through above analysis, following conclusions could be summarized:

(1)In consequence of studies, soil index properties tightly related to the collapsibility coefficient were determined as void ratio(e), dry density(ρ_d), plasticity index(I_p), water content(w) and degree of saturation(S_r).

(2)The HHO algorithm could optimize the initial values of the threshold and connection weight in BP neural network so as to significantly improve the convergence speed and prediction accuracy. Comparative analysis of correlation coefficients, the results show that the HHO-BP network model could significantly improves the prediction accuracy and operation speed compared with the BP neural network and PSO-BP network model. The five-parameter model includes the main factors that affect the coefficient of collapsibility comprehensively and has higher prediction accuracy and less error than the four-parameter model.

(3)Through the sensitivity analysis of the loess coefficient of collapsibility by the connection weight method, it is found that the void ratio and plasticity index have a great influence on the collapsibility coefficient, followed by dry density, and degree of saturation, while the water content has the least effect.

(4) In the testing stage, the comparison between the predictions of the 5-parameter HHO-BP model and the experimental results shows that R^2 values are higher than 0.9, RMSE and MAE values are as low as 0.005 and 0.0039. The results are satisfactory. Therefore, instead of the expensive, time-consuming and difficult experiments, it is highly suggested to use the 5-parameter HHO-BP neural network model for the preliminary prediction of the collapsibility coefficient in practical engineering.

Acknowledgments

This research was funded by the Key research Project of higher education institutions in Henan Province (Grant NO. 23B560011) and the Key Science and Technology Research Projects of Henan Province (Grant NO. 232102321002). Besides, it was funded by Research Fund for high level talents of Luoyang Institute of Science and Technology (Grant NO. 21010625).

References

[1] Li Y.R., Shi W.H., Aydin A., Beroya-Eitner M. A., and Gao G. “Loess genesis and wordwide distribution,” Earthscience Reviews, Vol.201, Article ID 102947, 2020.

[2] Liu Y.D., Yang Y.D., Dong Y.X., Lv Y.F., Wang D. and Qi L. “Mechanical properties and Microstructure Characteristics of the Loess Modified by the Consolid System,” Advances in materials Science and Engineering, Vol 2022, Article ID 1629895, 2022. https://doi.org/10.1155/2022/1628985

[3] Roberts, H.M., Muhs, D.R. and Bettis Iii, E.A. Loess Records | North America. In: Editor-in-Chief: Scott, A.E. (ed.) “Encyclopedia of Quaternary Science,” Elsevier, Oxford, pp.1456-1466. 2007.

[4] Nie Y.P., Ni W.K., Wang H.M., Yuan K.Z., Tuo W.X., Li X.N. “Evaluation of Collapsibility of Compacted Loess Based on Resisitivity Index,” Advances in Materials Science and Engineering, vol. 2021, Article ID 9990012, 2021. https://doi.org/10.1155/2021/9990012

[5] Wang, Sadeghi H, Hossen SK B, Chiu C.F., Alonso E. E, Baghbanrezvan S. “Water retention and volumetric characteristics of intact and re-compacted loess,” Journal of Canadian Geotechnical. Vol. 53, no. 8, 2013. https://doi.org/10.1139/cgj-2015-0364

[6] Liu Z, Liu F Y, Ma F L, Wang M, Bai X H, Zheng Y L, Yin H, Zhang G P. “Collapsibility, composition, and microstructure of a loess in China,” Journal of Canadian Geotechnical. Vol. 54, no. 4, pp. 673-686, 2016. https://doi.org/10.1139/cgj-2015-0285

[7] Xie W L, Li P, Vanapalli S K, Wang J D. “Prediction of the wetting-induced collapse behavior using the soil-water characteristic curve,” Journal of Asian Earth Science. Vol. 151, pp. 259-268. 2018. https://doi.org/10.1016/j.jseaes.2017.11.009

[8] Li P, Vanapalli S K, Li T L. “Review of collapse triggering mechanism of collapsible soils due to wetting,” Journal of Rock Mechanics and Geotechnical Engineering, Vol. 8, pp. 256-274, 2016. https://doi.org/10.1016/j.jrmge.2015.12.002

[9] An P, Zhang A J, Xing Y CH, Zhang B, Ni W K, Ren W Y. “Experimental study characteristics of thick self-weight collapsible loess in Xinjiang Ili region in China using field immersion test,” Soils and Foundation, Vol. 58, pp. 1476-1491, 2018. https://doi.org/10.1016/j.sandf.2018.08.005

[10] Wu X P, Zhao Y H, Xu A H, Mi W J, Zhao S Q. “Relationship between Collapsibility and Physical-mechanical Indexes of Loess and Evaluation Methods,” Chinese Journal of Yangtze River Scientific Research Institute, Vol. 35, no. 06, pp. 75-80. 2018. DOI: 10.11988/ckyyb.20170160

[11] Reznik Y. M. “Influence of physical properties on deformation characteristics of collapsible soils,” Engineering Geology, Vol. 92, no. 11, pp.27-37, 2007.

[12] Francisca F. M. “ Evaluating the constrained modulus and collapsibility of loess from standard penetration test,” International Journal of Geomechanics, Vol.7, no.4, pp. 307-310, 2007. 10.1061/(ASCE)1532-3641(2007)7:4(307)

[13] Gaaver K. E. “Geotechnical properties of Egyptian collapsible soils,” Alexandria Engineering Journal, Vol.51, no. 3, pp. 205-210, 2012. http://dx.doi.org/10.1016/j.aej.2012.05.002

[14] Wang J Q, Lei S. Y, Li X L, Wang Y M, Liu Z, Wang X G. “Correlation of wet collapsibility coefficient and physical property parameters of loess,” Coal geology & exploration, Vol. 41, no. 3, pp. 42-50, 2013. DOI: 10.3969/j.issn.1001-1986.2013.03.010

[15] Shu Z L, Zhu SH C, Jiang H. “Correlation analysis between collapsibility characteristics and physical properties of loess,” Water Power. Vol. 46, no. 11, pp. 120-124, 2020.

[16] Zhang, S. H. . "A Method of Collapsibility Classification Based on Probabilistic Neural Network." Computer Science & Service System (CSSS), 2012 International Conference on IEEE Computer Society, 2012.

[17] Salehi T., Shokrian M., Modirrousta A., Khodabandeh M., Heidari M., “ Estimation of the collapse potential of loess soils in Golestan Province using neural networks and neuro-fuzzy systems,” Arabian Journal of Geosciences, Vol. 8, pp.9557-9567, 2015.

[18] Zhu F J, Nan J J, Wei Y Q, Bai L. “Mathematical statistical analysis on factors affecting collapsible coefficient of loess,” Chinese Journal of Geological Hazards and Prevention, Vol. 39, no. 2, pp. 128-133, 2019. DOI: 10.16031/j.cnki.issn.1003-8035.2019.02.17

[19] Gao L X, Luan M T, Yang Q. ”Evaluation of loess collapsibility based on principal components of microstructural parameters,” Chinese Journal Rock of Soil Mechanics, Vol. 33, no. 7, pp. 1921-1926, 2012.

[20] Li L J, Zhao T Y, Li J. “Collapsibility and physical and mechanical characteristics of loess in Gansu Corridor,” Engineering Survey, Vol. 46, no. 3, pp. 22-28, 2018.

[21] Basma, A.A., Kallas, N. “Modeling soil collapse by artificial neural networks,” Geotechnical and Geological Engineering, Vol. 22, pp. 427–438, 2004. https://doi.org/10.1023/B:GEGE.0000025044.72718.db

[22] An N. “Prediction of loess collapsibility based on BP neural network,” Subgrade Engineering. no.1, pp.72-73, 2009.

[23] Feng X D. Evaluation of Loess Collapsibility for the Foundation of a Simulation Dam. Master's Thesis. Lanzhou University. Gansu, China. 2012.

[24] Su R, Wang X, Jiang D J, Liu D, He F, Han G X. “Study on Prediction Model of Loess Collapsibility Coefficient Based on BP Neural Network with Constraint,” Subgrade Engineering, no. 3, pp.14-18, 2019. DOI: 10.13379/j.issn.1003-8825.2019.03.03

[25] Zhan H Z, Lin J F. “Application of BP Neural Network in Prediction Collapsibility Coefficient of Loess,” Soil Engineering and Foundation, Vol. 34, no. 4, pp.493-496, 2020.

[26] Li P, Xie W L, Rnoald Y.S. Pak, Vanapalli S K. “Microstructural evolution of loess soils from the Loess Plateau of China,” Catena. Vol. 173, pp. 276-288, 2019. https://doi.org/10.1016/j.catena.2018.10.006

[27] Li X A, Li L C, Song Y X, Hong B, Wang L, Sun J Q. “Characterization of the mechanisms underlying loess collapsibility for landcreation project in Shananxi Province, China-a study from a micro perspective,” Engineering Geology, Vol. 249, pp.77-88, 2019. https://doi.org/10.1016/j.enggeo.2018.12.024.

[28] Wei Y N, Fan W, Yu B, Deng L S, Wei T T “Characterization and evolution of three-dimensional microstructure of Malan loess,” Catena, Vol. 192, Article ID.104585, 2020. https://doi.org/10.1016/j.catena.2020.104585

[29] Ye W M, Cui Y J, Huang Y., Delage P. “Collapsibility of Loess and its Discrimination Criteria,” Chinese Journal of Rock Mechanics and Engineering. Vol. 25, no. 3, pp.550-556, 2006.

[30] Sadeghi H., Kiani M., Sadeghi M., Jafarzadeh F. “Geotechnical characterization and collapsibility of a natural dispersive loess,” Engineering Geology, Vol.250, pp. 89-100, 2019. doi:10.1016/j.enggeo.2019.01.015

[31] Wang L. Q., Shao S. J. She F. T. “A new method for evaluating loess collapsibility and its application,” Engineering Geology, Vol. 264 Article ID. 105376, 2020. 10.1016/j.enggeo.2019.105376

[32] Hedari A A, Mirjalili S, Faris H, et al. “Harris hawks optimization: algorithm and applications,” Future Generation Computer Systems, Vol. 97, pp. 849-872, 2019. https://doi.org/10.1016/j.future.2019.02.028

[33] Alabool H. M., Alarabiat D., Abualigah L., Heidar A. A. “Harris hawks optimization: a comprehensive review of recent variants and applications,” Neural Computing and Applications. Vol. 33, no.15, pp. 8939-8980, 2021. https://doi.org/10.1007/s00521-021-05720-5

[34] Wang M. “Study on structure of collapsible loess in china,” Master's Thesis. Taiyuan University of Technology. Shanxi, China. 2010.

[35] Ding W. F.” Study on the collapsible zoning of loess along the second phase of the Han-Ji-Yi River Diversion Project,” Master's Thesis. Xi’an University of Science and Technology, Shanxi, China. 2020.

[36] Liu C. L. “Formation of Negative skin friction and its time effect of Single pile,” Master's Thesis. Chang’an University, Shanxi, China. 2004.

[37] Han Q. “The research on the loess collapsibility of the first subway in Xi’an,” Master's Thesis. Xi’an University of Technology, Shanxi, China. 2010.

[38] Erkan O, Isik B, Cicek A, Kara F. “Prediction of Damage Factor in end Milling of Glass Fibre Reinforced Plastic Composites Using Artificial Neural Network,” Appl Compos Mater, Vol. 20, pp. 517-536, 2013. DOI 10.1007/s10443-012-9286-3

[39] Essa F.A., Mohamed Abd Elaziz, Ammar H. Elsheikh. “An enhanced productivity prediction model of active solar still using artificial neural network and Harris Hawks optimizer,” Appiled Thermal Engineering, Article ID: 115020, 2020 https://doi.org/10.1016/j.applthermaleng.2020.115020

[40] Zhang Y, Zhang X M, Zhou Z J. “Analysis of Loess Collapsibility and the influence Factors,” Highway, Vol. 65, no. 8, pp. 69-75, 2020.